Site-Directed Mutagenesis of Dimethyl Sulfoxide Reductase from *Rhodobacter capsulatus*: Characterization of a Y114 → F Mutant†

Justin P. Ridge,‡ Kondo-Francois Aguey-Zinsou,§ Paul V. Bernhardt,§ Ian M. Brereton,|| Graeme R. Hanson,|| and Alastair G. McEwan*,‡

Centre for Metals in Biology, Department of Microbiology and Parasitology, Department of Chemistry, School of Molecular and Microbial Sciences, and Centre for Magnetic Resonance, University of Queensland, St. Lucia, Queensland 4072, Australia

Received August 15, 2002; Revised Manuscript Received October 27, 2002

ABSTRACT: A system for expressing site-directed mutants of the molybdenum enzyme dimethyl sulfoxide reductase from *Rhodobacter capsulatus* in the natural host was constructed. This system was used to generate and express dimethyl sulfoxide reductase with a Y114F mutation. The Y114F mutant had an increased k_{cat} and increased K_m toward both dimethyl sulfoxide and trimethylamine *N*-oxide compared to the native enzyme, and the value of k_{cat}/K_m was lower for both substrates in the mutant enzyme. The Y114F mutant, as isolated, was able to oxidize dimethyl sulfide with phenazine ethosulfate as the electron acceptor but with a lower k_{cat} than that of the native enzyme. The pH optimum of dimethyl sulfide: acceptor oxidoreductase activity in the Y114F mutant was shown to be shifted by +1 pH unit compared to the native enzyme. The Y114F mutant did not form a pink complex with dimethyl sulfide, which is characteristic of the native enzyme. The mutant enzyme showed a large increase in the K_d for DMS. Direct electrochemistry showed that the Mo(V)/Mo(IV) couple was unaffected by the Y114F mutant, but the midpoint potential of the Mo(VI)/Mo(V) couple was raised by about 50 mV. These data confirm that the Y114 residue plays a critical role in oxidation−reduction processes at the molybdenum active site and in oxygen atom transfer associated with sulfoxide reduction.

Molybdenum-containing enzymes, with the exception of nitrogenase, form a large but coherent group of enzymes found in all forms of life (*1*). The common feature of all these enzymes is the presence of a pterin molybdenum cofactor (Moco)[1] in which a Mo atom is coordinated by one or two ene−dithiolate ligands arising from an organic moiety known as molybdopterin (MPT) (*2*). The dimethyl sulfoxide reductase family of MPT-containing enzymes is distinguished by the presence of MPT in a dinucleotide form and the coordination of Mo by two molybdopterin guanine dinucleotide (MGD) groups (reviewed in refs *3* and *4*). Enzymes of the DMSO reductase family are only found in prokaryotes where they have a particularly important role in anaerobic respiration and lithotrophy (*5*). The X-ray crystal structures of several members of the DMSO reductase family have been solved: periplasmic DMSO reductase (*6*−*10*), formate dehydrogenase (FDH) (*11*), periplasmic nitrate reductase (NAP) (*12*), trimethylamine *N*-oxide (TMAO) reductase (*13*), and arsenite oxidase (ASO) (*14*). These structures showed that the enzymes of this family exhibit a highly conserved four-domain tertiary structure (*4*, *5*). There are, however, some differences seen between members of this family. The most obvious of these is the presence of an [Fe-S] cluster in FDH, NAP, and ASO which is absent in DMSO reductase and its close relative TMAO reductase from *Shewanella massilia*.

The common structural features of enzymes of the DMSO reductase family raise the question of how substrate specificity and kinetic properties are determined. It seems likely that this is related to differences in the structure of the Mo active site and its immediate environment. The two dithiolenes coordinating the Mo form a distorted square-planar base while the Mo is capped by ligands in a trigonal prismatic arrangement. Apart from ASO, in enzymes of the DMSO reductase family one of these ligands is provided by a nearby amino acid side chain, a serine in the case of DMSO reductase (*6*) and TMAO reductase (*13*), cysteine in the case of NAP (*12*), and selenocysteine in the case of FDH (*11*). In addition to the MPT-based and protein-based ligands, other

† This work was supported by a grant from the Australian Research Council to A.G.M. and G.R.H.

* Corresponding author. Telephone: +61 (0)7 33654878. Fax: +61 (0)7 33654820. E-mail: mcewan@uq.edu.au.

‡ Department of Microbiology and Parasitology, University of Queensland.

§ Department of Chemistry, School of Molecular and Microbial Sciences, University of Queensland.

|| Centre for Magnetic Resonance, University of Queensland.

[1] Abbreviations: *Rb.*, *Rhodobacter*; Moco, pterin molybdenum cofactor; MPT, molybdopterin; MGD, molybdopterin guanine dinucleotide; DMSO, dimethyl sulfoxide; DMS, dimethyl sulfide; TMAO, trimethylamine *N*-oxide; TMA, trimethylamine; DMSOR, dimethyl sulfoxide reductase; FDH, formate dehydrogenase; NAP, periplasmic nitrate reductase; ASO, arsenite oxidase; TMAOR, trimethylamine *N*-oxide reductase; Gm, gentamicin; Km, kanamycin; SDS−PAGE, sodium dodecyl sulfate−polyacrylamide gel electrophoresis; NBT/BCIP, nitro-blue tetrazolium chloride/5-bromo-4-chloro-3-indolyl phosphate toluidine; PCR, polymerase chain reaction; MV, methylviologen; PES, phenazine ethosulfate; DCPIP, dichlorophenolindophenol; MES, 4-morpholinoethanesulfonic acid; CHES, 2-(cyclohexylamino)ethanesulfonic acid; CAPS, 3-(cyclohexylamino)-1-propanesulfonic acid; NMR, nuclear magnetic resonance.

10.1021/bi0266582 CCC: $22.00
Published on Web 12/03/2002

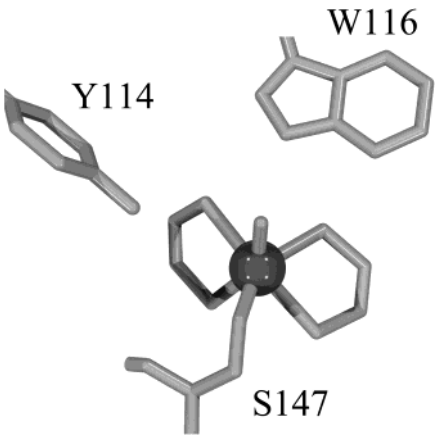

FIGURE 1: Environment surrounding the Mo(VI) center in DMSO reductase adapted from the X-ray crystal structure of DMSOR from *Rb. capsulatus* (*8*). The MGD moieties have been truncated for clarity. The Mo atom is shown in a darker shade. The amino acid side chains have been labeled using single letter codes and position relative to the N-terminus.

ligands can be seen coordinated to the Mo. These are oxygen atoms (or oxo groups) and hydroxo (OH) or aqua (OH_2) groups. The presence of a single oxo group coordinated to Mo in the resting form of DMSO reductase which is exchanged during catalytic turnover is consistent with isotope exchange data measured using Raman spectroscopy (*15*, *16*). A notable distinguishing feature of DMSO reductase and TMAO reductase is the presence of potential hydrogen-bonding amino acid side chains close to the Mo active site. In DMSO reductase there are two nearby amino acid residues, Y114 and W116, which could form a hydrogen-bonding interaction with the oxo ligand of the Mo (Figure 1). This contrasts with the situation in other members of the DMSO reductase family. In NAP no H-bonding amino acids are within 3.5 Å of the single aqua ligand (*12*), in ASO only a single residue (K385) could hydrogen bond to the single oxo ligand (*14*), and in FDH_H no H-bonding residues were seen close to the hydroxo ligand of the oxidized structure (*11*). Despite differences in the description of the structure of the Mo active site in DMSO reductase, it is established that W116 is H-bonded to the single Mo−oxo group. This oxo group forms an adduct with dimethyl sulfide (DMS) and is presumed to be the site where DMSO binds to the Mo(IV) form during enzyme turnover (*9*).

The function of Y114 in DMSO reductase has been harder to establish. In the first structure of DMSO reductase from *Rhodobacter* (*Rb.*) *sphaeroides* (*6*) it was this residue that was suggested to H-bond to a single Mo−oxo group. In the seven-coordinate structure of DMSO reductase from *Rhodobacter capsulatus* two Mo−oxo groups were identified; oxo-1 which H-bonded to Y114 and oxo-2 which H-bonded to W116 (*8*). A five-coordinate dioxo Mo center in DMSO reductase from *Rb. capsulatus* was also described in which the thiolate from one of the MGD moieties was outside the Mo coordination sphere (*7*). Raman spectroscopic studies as well as EXAFS argue strongly against the presence of a second Mo−oxo group in DMSO reductase (*15*−*17*). More recently, analysis of a 1.3 Å resolution structure of DMSO reductase from *Rb. sphaeroides* has revealed that the Mo is discretely disordered (*10*). The Mo center exists in a six-coordinate monooxo form in which a single oxo group is H-bonded to W116 and a five-coordinate dioxo form which corresponds to a species described by Hüber and co-workers for DMSO reductase from *Rb. capsulatus* (*7*). Li et al. (*10*) have suggested that at a lower resolution (1.8 Å) a combination of these two species could have been interpreted as a seven-coordinate dioxo Mo(VI) species (*8*).

Despite the probability that no oxo-1 is present in DMSO reductase, it seems likely that Y114 plays an important role in the catalytic mechanism of the enzyme. It has been noted that in TMAO reductases, which are specific for *N*-oxides and cannot reduce *S*-oxides, Y114 is replaced by a serine or threonine residue (*13*). This led to the hypothesis that Y114 was critical for the control of substrate specificity in the *S*-oxide/*N*-oxide reductases. To test this hypothesis, Johnson and Rajagopalan (*18*) used site-directed mutagenesis to produce Y114 → F and Y114 → A mutants of DMSO reductase from *Rb. sphaeroides*. This study showed that these substitutions altered the UV−visible spectra of DMSO reductase and its catalytic properties toward a variety of substrates. The recombinant *Rb. sphaeroides* DMSO reductase is expressed in *Escherichia coli* as a histidine-tagged protein and is assembled in the cytoplasm (*19*). Although Moco is inserted into the enzyme, it is inactive until it is reductively conditioned by catalytic turnover using dithionite-reduced methyl viologen plus DMSO. The potential for structural alterations to the Mo active site is well established, and this suggested that expression in *E. coli* may not be the optimal method for analysis of periplasmic enzymes of the DMSO reductase family (*20*). In this paper we describe an expression system that allows DMSO reductase to be expressed in *Rb. capsulatus*. This produces recombinant enzyme that has followed an identical pathway of biogenesis as the native enzyme, resulting in its translocation to the periplasm. We have used this system to produce and analyze a Y114 → F mutant, and we report herein its structural and catalytic properties.

EXPERIMENTAL PROCEDURES

Construction of a Δ*dorA Strain of Rb. capsulatus.* A portion of the *dor* operon of *Rb. capsulatus* strain 37b4 (*21*) from residue 293 of *dor*C to downstream of *dor*B was cloned into pUC19 as a 3.8 kbp *Bam*HI fragment to give the plasmid pUCJRDor. This clone contained the entire *dorD* and *dorA* genes. An internal 1.4 kbp *Eco*RI fragment of *dor*A was then removed, and a gentamicin (Gm) resistance cassette derived from pR440 (*22*) was cloned in its place to give the plasmid pUCΔ*dor*A. The *Bam*HI fragment containing the mutated *dorA* gene was then released from pUCΔ*dor*A and cloned into the plasmid pJP5603 (*23*) to produce the plasmid pJP5603Δ*dor*A. The conjugative strain of *E. coli*, S17-1 λpir, was then transformed with pJP5603Δ*dor*A, and the resultant strain was used to introduce pJP5603Δ*dor*A into *Rb. capsulatus* 37b4 through conjugative transfer using standard techniques (*24*). Resultant Gm^RKm^S clones of *Rb. capsulatus* were screened for DMSO reductase by Western blotting. Potential mutants were grown in RCV media under photrophic anaerobic growth conditions in the presence of 15 mM DMSO. Total soluble protein was then obtained by incubation of the cells in the presence of lysozyme at 37 °C for 30 min followed by boiling for 10 min. Insoluble particles and whole cells were pelleted by centrifugation at 12000*g* for 2 min; 10 μL of the resultant supernatant was loaded onto a SDS−PAGE gel for the Western blot. Genomic DNA

was isolated from those strains which lacked *dor*A using DNAzol (Gibco) following the manufacturer's protocol. Primers external to the deleted region of *dorA* were then used to amplify the region containing the Gm cassette. The resultant product had an approximate size of 3.0 kb, compared to a product from the wild-type gene of 1.8 kb, indicating the correct insertion of the Gm cassette. This strain was named 37b4Δ*dor*A.

Mutagenesis and Expression of dorA. The plasmid pUCJRDor was used as the template for site-directed mutagenesis. Mutant *dorA* genes were generated using the QuikChange XL site-directed mutagenesis kit (Stratagene) following the manufacturer's protocol. For generation of the Y114 → F mutant the primers used were Y114Ffwd, 5′CTTTGGCGGCTCCTTCGGCTGGAAAAGC3′, and Y114Frev, 5′GCTTTTCCAGCCGAAGGAGCCGCCAAAG3′. Resultant clones were screened by sequencing the coding region encompassing Y114. Three positive clones were then selected, and the entire *Bam*HI fragment in each was sequenced to ensure that no other changes had been introduced. In all three cases no other changes were introduced, and so one clone was selected for further cloning. The *Bam*HI fragment from this clone was then cloned into pJP5603 to give the plasmid, pJP5603Y114F. This plasmid was then used to transform S17-1 λpir and the resulting strain used for conjugation with 37b4Δ*dor*A. Resultant Gm^RKm^R clones were then screened for production of DMSO reductase via Western blotting as described above with the exception that DMSO was only added after the cells had reached stationary phase, and then incubation was continued for a further 8 h. Genomic DNA was then isolated from the positive clones, as above. PCR was then used to amplify the region encompassing the central portion of *dor*A, which was then sequenced to confirm the presence of the mutation. A positive strain was selected for further study and named 37b4Y114F.

Purification of DMSO Reductase. Purification of mutated DMSO reductase was carried out essentially as previously described (*25*). Cells were harvested by centrifugation at 3800*g* for 40 min. The resultant cell pellet was then washed in at least 2 × 1 L of 50 mM Tris-HCl (pH 8.0). The periplasmic fraction was then isolated by incubation of the cells in spheroplast buffer [50 mM Tris-HCl (pH 8.0), 0.5 M sucrose, 1.5 mM EDTA] with 500 mg/L lysozyme at 30 °C for 30 min with occasional agitation. The spheroplasts were then removed by centrifugation at 9000*g* for 30 min. Ammonium sulfate was then added to the supernatant to 50% saturation and the precipitate formed removed by centrifugation at 9000*g* for 30 min. The supernatant was then recovered and additional ammonium sulfate added to 75% saturation. The precipitate was recovered as above, the supernatant discarded, and the pellet resuspended in 15% $(NH_4)_2SO_4$/50 mM Tris-HCl (pH 8.0). This solution was then loaded onto a phenyl−Sepharose Fast-Flow self-packed column (Pharmacia) preequilibrated with 15% $(NH_4)_2SO_4$/50 mM Tris-HCl (pH 8.0). A gradient of decreasing ammonium sulfate was then used to elute the protein. SDS−PAGE analysis was used to identify the fractions containing the DMSO reductase. Those fractions containing DMSO reductase were pooled and concentrated using a pressurized ultrafiltration cell (Amicon). The enzyme was then further purified using a size-exclusion column (Sephacryl 200, Pharmacia) followed by an anion-exchange column (POROS 20HQ, PerSeptive Biosystems). Each time SDS−PAGE was used to identify the fractions containing DMSO reductase.

Kinetic Analysis. Steady-state kinetic measurements of MV:DMSO oxidoreductase activity and PES-dependent DMS:DCPIP oxidoreductase activity were measured as described previously (*25*). Determination of k_{cat} and K_m values were carried out in triplicate. Values of k_{cat} are expressed as moles of DCPIP or reduced MV consumed per mole of enzyme per second giving units of s^{-1}. The pH dependence of DMS oxidation was determined by measurement of k_{cat} at ∼0.5 pH intervals between pH ∼5.5 and pH ∼10.4. The buffers used were 25 mM MES (pH 5.5), 25 mM MES (pH 6.0), 25 mM MES (pH 6.5), 50 mM Tris-HCl (pH 6.9), 50 mM Tris-HCl (pH 7.5), 50 mM Tricine (pH 8.0), 50 mM Tricine (pH 8.5), 50 mM CHES (pH 9.0), 50 mM CHES (pH 9.5), 50 mM CAPS (pH 10.0), and 50 mM CAPS (pH 10.4), using HCl or NaOH to set the correct pH. All steady-state kinetic data generated were fitted using the regression analysis within the Sigma Plot 2000 program (SPSS).

Optical Spectroscopy. All UV−visible spectroscopy was carried out using a Hitachi U3000 spectrophotometer. Data for determination of dissociation constants were fitted using the regression analysis within the Sigma Plot 2000 program (SPSS).

Direct Electrochemistry. The midpoint potentials of the Mo(VI)/Mo(V) and Mo(V)/Mo(IV) couples of the Mo center were determined with cyclic voltammetry using equipment as described in ref *26*. A clean electrode surface was obtained by cleaving a ca. 1 μm layer from the face of an edge plane pyrolytic graphite working electrode (0.03 cm^2) with a microtome followed by sonication in distilled water. No abrasives were used. A surfactant film of the enzyme was prepared as follows. A solution of protein (10 μL, 332 μM) was combined with a 15 μL solution comprising didodecyldimethylammonium bromide (DDAB, 2 mM) and Tris-HCl buffer (50 μM). The working electrode surface was coated with this mixture and then allowed to dry overnight at 6 °C. The solution volume was ca. 500 μL, and the pH was varied from 5 to 10 using the buffer mixture of bis-tris propane (10 mM) and 2-amino-2-methylpropan-1-ol (10 mM), with 0.01 M NaCl as supporting electrolyte.

Measurement of DMSO Respiratory Activity in Whole Cells Using NMR. The rate of DMS or TMA production by whole cells of both wild-type and Y114F strains was monitored using NMR spectroscopy essentially as described in ref *27*. Briefly, cells grown under inducing conditions were recovered by centrifugation for 10 min at 3800*g*. The cells were then washed twice in malate-free RCV media. The cells were then resuspended in malate-free RCV to give an OD_{600} of approximately 0.5. These cells were then placed in a NMR tube, and D_2O was added to a final concentration of 4%. DMSO or TMAO was added to final concentrations of 15 and 60 mM, respectively. The 500 MHz ^1H NMR spectra at 25 °C were recorded using a Bruker Avance 500 spectrometer and a 5 mm triple resonance (^1H, ^{15}N, ^{13}C) probe head. A spectrum of the sample was then taken every 2 min for a total time of 40 min in each case. The level of product was calculated from the increase in the area of the peak centered at either 2.11 ppm for DMS or 2.88 ppm for TMA. The area was estimated from the fitting of a Lorentzian peak to the data.

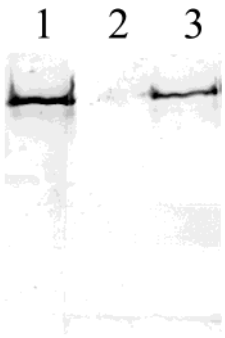

FIGURE 2: Western blot of periplasmic extracts of *Rb. capsulatus* strains using polyclonal antibodies raised against DMSO reductase. Lanes: 1, 37b4; 2, 37b4ΔdorA; 3, 37b4Y114F.

RESULTS

Development of a Method for Expression of Site-Directed Mutants in Rb. capsulatus. Development of a genetic system for expression of site-directed mutants in *Rb. capsulatus* required the deletion of the *dorA* gene from the host followed by its replacement with a mutated copy of this gene. The first step was achieved by marker exchange in which the wild-type *dorA* gene was replaced with a *dor* operon in which most of the *dorA* gene had been deleted and replaced with a Gm resistance cassette. This drug resistance cassette lacks a transcription terminator, resulting in read-through into the genes distal to *dorA*. This is critical for the expression system since the downstream *dorB* and the Moco biosynthetic genes are located here and they are essential for high-level expression of DMSO reductase (*21*, *28*). Figure 2 shows a Western blot of periplasmic extracts from *Rb. capsulatus*; in contrast to the situation in wild-type cells (lane 1) no DMSO reductase was produced in the Δ*dor*A mutant (lane 2). Although it might have been possible to express the *dorA* gene in trans from a replicative plasmid in the Δ*dor*A mutant, we chose to place the *dorA* gene back on the chromosome for expression. To achieve this, we made use of the fact that recombination by single crossover between the *dorA* gene and the copy of *dorA* interrupted with the Gm cassette was not possible. When the suicide plasmid containing the *dorA* gene was transferred to the Δ*dor*A mutant, a single crossover occurred in the *dorD* gene which lies upstream of *dorA*, and this results in the cotransfer of a complete *dorA* gene onto the chromosome. The resulting strain also contains the plasmid pJP5603 and hence is easily selected for by its resistance to kanamycin. Figure 2 (lane 3) shows that expression of the DMSO reductase polypeptide was restored in the construct described above. The recombinant DMSO reductase was exclusively located in the periplasm, as is the enzyme from wild-type cells (data not shown). The level of DMSO reductase activity in the periplasm of mutant cells (0.28 pmol of reduced MV consumed mg^{-1} min^{-1}), while lower than that of wild-type cells (0.58 pmol of reduced MV consumed mg^{-1} min^{-1}), was suitable for the investigation of site-directed mutants.

Characterization of a Y114F Mutant. A strain for expression of a Y114F mutant of DMSO reductase was constructed as described above. The presence of a mutation in the *dorA* gene following its incorporation onto the chromosome of the Δ*dor*A mutant was confirmed by PCR amplification of this region and DNA sequencing analysis. This analysis was carried out at first to confirm the validity of putative mutants,

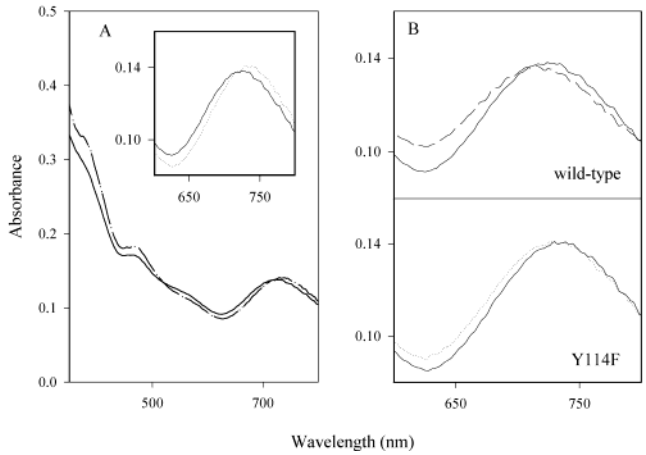

FIGURE 3: (A) UV−visible spectra of the as-prepared, oxidized forms of wild-type (solid line) and Y114F (dashed line) DMSO reductase of *Rb. capsulatus*. Inset: long-wavelength transitions of wild-type and Y114F DMSO reductase. (B) UV−visible spectra of the long-wavelength transitions of wild-type and Y114F DMSO reductase with (dashed line) and without (solid line) the addition of 20 mM DMSO.

and it was then used to confirm that no reversion had occurred during growth of the cells for production of DMSO reductase. Purification of Y114F DMSO reductase from periplasmic extracts proceeded in a manner identical to that of the wild-type enzyme. The yield of protein from 37b4Y114F was lower but comparable to that from the wild-type strain. The purified Y114F DMSO reductase was gray-brown in color, similar to the wild-type protein. SDS−PAGE and Western blot analysis showed the purified protein to be of identical size to the wild-type protein and react with an anti-DMSO reductase antibody.

UV−Visible Spectroscopy. UV−visible spectra of the resting Mo(VI) forms of native DMSO reductase and the Y114F mutant enzyme are shown in Figure 3A. In the near-UV/blue region of the spectrum only slight differences were seen in the region 340−400 nm where the shoulder seen in the spectrum of the native enzyme appears to have a more defined peak when compared to the spectrum of the Y114F mutant enzyme. A second difference can be seen in the longer wavelength electronic transition that is characteristic of the oxidized form of DMSO reductase. In native DMSO reductase a broad absorption band is observed which is centered at 725 nm. In the Y114F enzyme this transition is red shifted and is centered at 735 nm. This result contrasted with the description of the recombinant Y114F mutant of *Rb. sphaeroides* DMSO reductase expressed and purified from *E. coli* (*18*). In this case the oxidized Mo(VI) species had an absorption maxima, post-redox cycling, at 690 nm which was blue shifted compared to wild-type DMSO reductase. Comparison of these data suggested that there might be significant differences between the recombinant DMSO reductases expressed in distinct host organisms.

Binding of DMSO to the Mo(VI) Form of DMSO Reductase. Bray and co-workers have demonstrated that DMSO binds to the oxidized Mo(VI) form of DMSO reductase and causes a blue shift in the absorption maximum of the electronic transition associated with the 725 nm peak (*29*). Addition of DMSO to a concentration of 15 mM to the native enzyme caused a blue shift in the long-wavelength transition from 725 to 712 nm as described previously (Figure 3B). A

Table 1: Steady-State Kinetic Parameters Determined for the Wild-Type (WT) and Y114F DMSO Reductases from *Rb. capsulatus* for the Substrates DMSO, TMAO, and DMS

	MV:DMSO oxidoreductase			MV:TMAO oxidoreductase			PES-dependent DMS:DCPIP oxidoreductase		
	k_{cat} (s^{-1})[a]	K_m (μM)[b]	k_{cat}/K_m ($\mu M^{-1}\cdot s^{-1}$)	k_{cat} (s^{-1})[a]	K_m (μM)[b]	k_{cat}/K_m ($\mu M^{-1}\cdot s^{-1}$)	k_{cat} (s^{-1})[a]	K_m (μM)[b]	k_{cat}/K_m ($\mu M^{-1}\cdot s^{-1}$)
WT	42.9 ± 0.6	9.7 ± 1.2	4.4 ± 0.7	134.5 ± 4.9	193.8 ± 9.8	0.69 ± 0.07	2.8 ± 0.2	nd[c]	
Y114F	81.4 ± 2.4	185.5 ± 10.3	0.44 ± 0.037	378.7 ± 27.5	811.8 ± 24.6	0.47 ± 0.05	0.7 ± 0.1	nd	

[a] k_{cat} values are the mean of three determinations in each case (±SEM). [b] K_m values are derived from a linear fit of an Eadie−Hofstee plot of the average of three determinations at each substrate concentration (±SEM). [c] nd = not determined.

similar effect was seen upon the addition of an identical amount of DMSO to the Y114F DMSO reductase, the long-wavelength transition showing an apparent shift to 728 nm.

Steady-State Kinetic Analyses. DMSO reductase activity was measured using dithionite-reduced methyl viologen as an electron donor. The results in Table 1 show that the Y114F mutant enzyme had a higher k_{cat} toward both DMSO and TMAO compared to the native enzyme. However, this increased turnover number for the mutant DMSO reductase was more than compensated for by the higher K_m values for both DMSO and TMAO in the Y114F mutant enzyme compared to native DMSO reductase. Taken together, these data show that for the Y114F mutant enzyme there is a 10-fold decrease in the k_{cat}/K_m value for DMSO and a small decrease in the k_{cat}/K_m value for TMAO when compared to wild-type DMSO reductase. These results are similar to those described by Johnson and Rajagopalan (*18*) for the recombinant DMSO reductase from *Rb. sphaeroides* expressed in *E. coli*.

The plasticity of the Mo active site in DMSO reductase and the observation that inactive forms of the enzyme can easily be generated led Bray and co-workers (*30*) to propose that a better measure of an undamaged Mo active site in DMSO reductase is its ability to catalyze the oxidation of DMS in the PES-dependent DMS:DCPIP oxidoreductase assay. Johnson and Rajagopalan (*18*) reported that neither the wild type nor the Y114F mutant of recombinant DMSO reductase from *Rb. sphaeroides* expressed in *E. coli* had PES-dependent DMS:DCPIP oxidoreductase activity. However, when these enzymes were reductively conditioned by turnover with reduced methyl viologen plus DMSO, PES-dependent DMS:DCPIP oxidoreductase activity of both enzymes was restored, but in the Y114F mutant the level of activity was only 4% of that of the native enzyme. Table 1 shows that native DMSO reductase from *Rb. capsulatus* was active in the DMS:DCPIP oxidoreductase assay without redox cycling. Similarly, the Y114F mutant exhibited activity in the same assay although it was only about one-fourth that of the native enzyme. Redox cycling did not enhance the turnover number of native or mutant enzyme in this assay (data not shown). The volatility of DMS made it difficult to measure the K_m values for this substrate. Neither enzyme showed any measurable activity with trimethylamine (TMA) as a reductant.

Product Formation in Whole Cells. The rate of product formation by whole cells of the wild-type and Y114F strains using DMSO or TMAO as substrate was monitored over time using NMR spectroscopy. Using this approach the rate of DMS formation in the Y114F cells was seen to be approximately 1.9 times faster than that seen in wild-type cells.

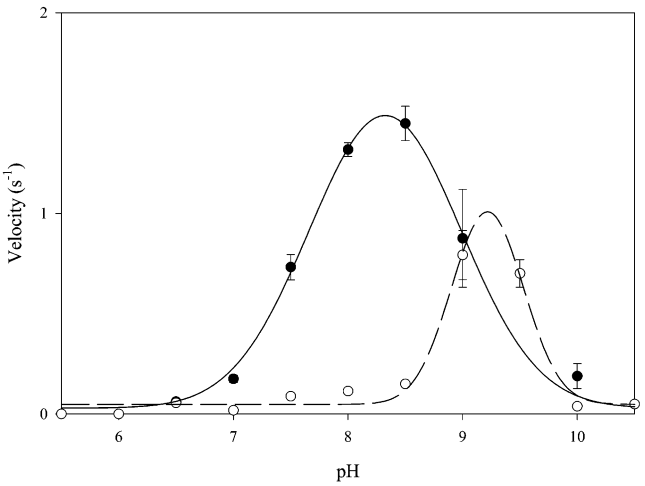

FIGURE 4: Plot of PES-dependent DMS:DCPIP oxidoreductase activity vs pH for both wild-type (solid line) and Y114F (dotted line) DMSO reductases.

The production of TMA by the same strains was also increased in the Y114F strain by a factor of approximately 1.7 (data not shown). The rate of TMA production was lower than that of DMS production in contrast to the data recorded for the purified enzyme.

pH Dependence of DMSO Oxidation. The rate of DMS oxidation by both wild-type and Y114F DMSOR was measured at ~0.5 pH intervals between ~pH 5.5 and ~pH 10.5 using the DMS:DCPIP oxidoreductase assay. For both the wild-type and Y114F DMSOR a well-defined peak of activity was observed, and very little activity was observed at lower pH values (Figure 4). Nonlinear regression analysis showed that in both cases a Gaussian distribution best fit the data ($r^2 > 0.93$). For the wild-type DMSO reductase the peak of activity was centered around pH 8.3 and had two pK_a values of 7.5 and 9.1. In contrast, the peak of activity for the Y114F DMSO reductase was considerably narrower and centered at about pH 9.2 with two pK_a values of 8.8 and 9.6.

Spectroscopic Studies of the Binding of DMS to DMSO Reductase. Addition of DMS to the wild-type enzyme to a final concentration of 8 mM altered the UV−visible spectrum of the enzyme. The long-wavelength transition was bleached, and two strong transitions centered at 480 and 550 nm, respectively, appeared, giving the enzyme a distinctive pink color. Further addition of DMS, up to a final concentration of 17 mM, to the wild-type enzyme caused no further changes in the spectrum. However, addition of DMS to the Y114F DMSO reductase did not give the distinctive pink form of the enzyme (Figure 5A). Changes in the UV−visible spectra of the Y114F enzyme still occurred following

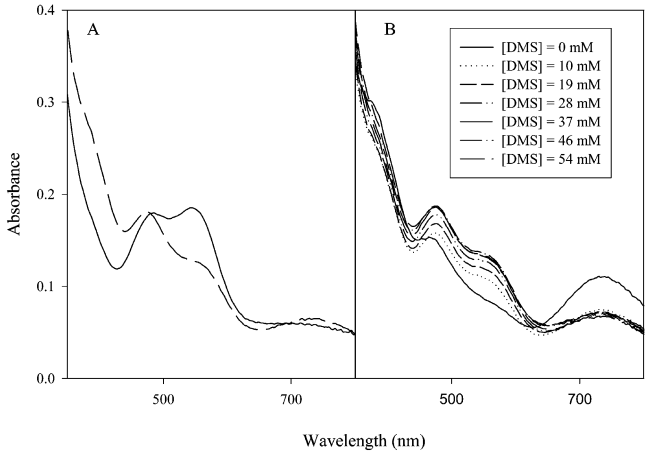

FIGURE 5: UV−visible spectra of wild-type and Y114F DMSO reductase showing the effect of the addition of DMS. (A) Wild type (solid line) and Y114F (dotted line) after addition of DMS. (B) Y114F DMSO reductase with increasing concentrations of DMS; see inset.

consecutive additions of DMS, reaching a final concentration of 55 mM (Figure 5B). These changes manifested themselves as an initial bleaching of the long-wavelength transition and appearance of weak transitions at 475 and 565 nm, respectively. Subsequent additions of DMS caused a strengthening of these two transitions but not to the level seen in the wild-type enzyme. The increase of the transition at 565 nm was monitored as a function of DMS concentration and yielded a dissociation constant for DMS of 19.09 ± 0.01 mM.

Electrochemistry of Y114F DMSO Reductase. Direct electrochemistry of Y114F DMSO reductase was carried out under nonturnover conditions. Our recent report of a non-turnover voltammetric response from the wild-type DMSO reductase of *Rb. capsulatus* showed the midpoint potentials of the Mo(VI)/Mo(V) and Mo(V)/Mo(IV) couples to be $E_{m,8}$ +161 mV and −102 mV vs NHE, respectively (*26*). The Mo(VI)/Mo(V) couple exhibited a pH dependence of ca. −59 mV/pH unit, consistent with a single electron/single proton transfer reaction. However, the redox potential of the Mo(V)/Mo(IV) couple was pH independent.

The midpoint redox potential of the Mo(VI)/Mo(V) couple in Y114F DMSO reductase was $E_{m,8}$ +229 mV and again displayed a pH dependence of approximately −59 mV/pH unit. At each pH point the Y114F DMSO reductase Mo(VI)/Mo(V) couple was consistently greater than the Mo(VI)/Mo(V) couple of the wild-type enzyme (Figure 6). The Mo(V)/Mo(IV) couple of Y114F DMSO reductase was again pH independent but lower than that measured for the wild type with a potential of $E_{m,8}$ −140 mV.

DISCUSSION

Previous studies of recombinant DMSO reductase by Rajagopalan and co-workers (*18*, *19*) have relied on expression of the enzyme from *Rb. sphaeroides* in an *E. coli*-based heterologous system. By removing the signal sequence from the *dorA* gene, it is possible to produce a recombinant enzyme containing Moco that is localized to the cytoplasm. However, these studies reported that the Mo active site of *Rb. sphaeroides* DMSO reductase synthesized in this system is not correctly assembled and requires reductive conditioning (redox cycling) before DMSO reductase activity can be

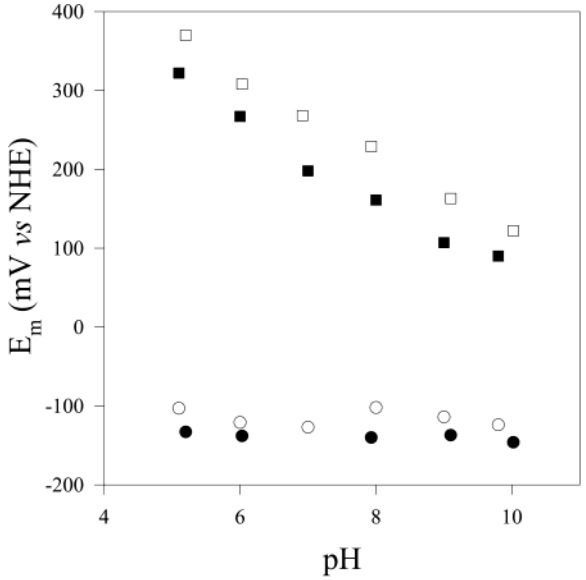

FIGURE 6: Plot of midpoint redox potentials of the Mo center in DMSO reductase vs pH. Mo(VI)/Mo(V) couple: wild type, closed squares; Y114F, open squares. Mo(V)/Mo(IV) couple: wild type, closed circles; Y114F, open circles. Errors are estimated to be 1−2 mV.

observed (*19*). The "as-isolated" recombinant form of DMSO reductase is green in color, and EXAFS studies suggested that it is a hexacoordinate dioxo form in which the methoxy side chain of S147 does not coordinate the Mo (*17*). Redox cycling converts the enzyme to a hexacoordinate monooxo form in which the serine acts as a ligand. In the homologous expression system described in this paper the *Rb. capsulatus* DMSO reductase is brown in color and is active in both the MV:DMSO oxidoreductase assay and PES-dependent DMS:DCPIP oxidoreductase assay without redox cycling. Even after redox cycling the PES-dependent DMS:DCPIP oxidoreductase activity of recombinant DMSO reductase from *Rb. sphaeroides* is low in comparison with the preparations from *Rb. capsulatus* described in this paper.

The suggestion that the active site in the *Rb. capsulatus* DMSO reductase expressed in its natural host may be different to the DMSO reductase expressed in *E. coli* is supported by the comparison of the UV−visible spectrum of the as-prepared, Mo(VI), form of the Y114F mutant DMSO reductase described above. The Y114F mutant of *Rb. sphaeroides* DMSO reductase expressed in *E. coli* shows a blue-shifted absorbance maximum relative to the 720 nm absorption band in the native enzyme while the same absorption band is red shifted in the Y114F mutant of *Rb. capsulatus*. This long-wavelength transition is sensitive to the coordination environment of the Mo center (*20*). The differences in visible absorption spectra seen between the Y114F mutant of *Rb. capsulatus* and that of *Rb. sphaeroides* would therefore imply that there are subtle differences in the Mo coordination sphere of the two enzymes. Whether these differences are a consequence of the method of expression of the recombinant enzymes or whether they reflect differences between the enzymes from the two *Rhodobacter* species still needs to be established.

Despite the differences seen in the spectra of the oxidized enzymes the kinetic data for both of the Y114F enzymes follow similar trends. In both cases a marked increase in k_{cat} was seen toward both DMSO and TMAO. This trend was

also seen in whole cells, implying that the interaction of Y114F DMSO reductase with the electron transport chain of *Rb. capsulatus* was not hindered by the amino acid substitution. However, for both enzymes this increase in k_{cat} is offset by a large increase in the K_m values. The value of k_{cat}/K_m can therefore be more representative of the overall efficiency of the enzyme. Using this measure the Y114F DMSO reductase of *Rb. capsulatus* is 10-fold less efficient at reducing DMSO and slightly less efficient at reducing TMAO. The decrease in the ability of the enzyme to reduce DMSO caused by the Y114F mutation is perhaps unsurprising as, as outlined previously, this residue appears to be a significant difference between the closely related DMSO reductases and the TMAO reductases (*18*). It is therefore quite reasonable to expect this residue to play a role in the reduction of *S*-oxides. Support for this view comes from the observation that the critical active site tyrosine is also present in biotin sulfoxide reductase (*18*). However, the Y114F mutation does not enhance the efficiency of TMAO reduction in the DMSO reductase of *Rb. capsulatus*, which is in contrast to the Y114F DMSO reductase of *Rb. sphaeroides* where a significant increase in the efficiency of TMAO reduction was seen. The authors also note that the reported values for the k_{cat} of the recombinant wild-type and Y114F *Rb. sphaeroides* DMSOR are considerably higher than the values found for the DMSO reductases of *Rb. capsulatus* (*18*). The critical differences in the active sites between DMSO reductases and TMAO reductases probably relate to differences in the properties of the substrates; the bond energy order of S−O is higher than N−O, and hence it is expected that the *N*-oxide will have higher reactivity (*31*, *32*).

The mechanistic pathway for reduction of *S*-oxides and *N*-oxides involves formation of a Mo(IV)−OX (X = S, N) bond and bond weakening of the substrate. The crystal structure of *Rb. capsulatus* DMSO reductase with DMSO bound at the active site and Mo K-edge near-edge X-ray absorption spectra of this complex show a Mo(IV) species in which the S−O bond of the bound DMSO molecule is weakened. The K_d for DMS in Y114F DMSO reductase increased by a factor of approximately 100-fold, when compared to the previously reported value of 0.16 mM for the wild-type enzyme (*29*). Since the reaction measured is the back-reaction with the product DMS, it suggests that this is providing information about the electron transfer/product release step in the mechanistic pathway of oxygen atom transfer from DMSO to Mo(IV). Our data suggest that the inability of the Y114F mutant enzyme to form the Mo(IV) species of DMSO reductase with DMSO bound is consistent with a critical role for this residue in the formation of a transition state that is linked to the generation of this intermediate.

Recently, density functional calculations (*33*) using model systems have led to the proposal that oxygen atom transfer and breakage of the O−S bond in DMSO bound at the Mo(IV) active site are facilitated by an interaction between a methoxy group, equivalent to that of S147 in the crystal structure. These calculations led to the proposal that in DMSO reductase the rigidity of the pterin ligands and positioning of the serine ligand result in an active site structure that closely resembles the freely optimized transition state for oxygen atom transfer from the substrate to the metal center. In the crystal structure of the Mo(IV) form of DMSO reductase with DMSO bound, we note that the distance between the sulfur atom of the DMSO and the Y114 −OH is only (3.3 Å) (*9*). Hence, the hydroxyl group of Y114 may also have a critical role in O−S bond weakening as a consequence of its interaction with the sulfur of DMSO.

The protein film voltammetry study of DMSO reductase confirms that Y114 plays a role in determining the electrochemical properties of Mo center and is critical for protonation steps at the active site. Direct electrochemistry of the Y114F mutant showed that the mutation had only influenced the Mo(VI)/Mo(V) couple, increasing this midpoint of this redox couple by about 50 mV. The second Mo(V)/Mo(IV) couple remained relatively unaffected by the mutation. We have previously shown that the redox potential for reduction of Mo(VI) to Mo(V) becomes pH independent at higher pH with a pK_a for the hydroxo−Mo(V) complex of about 9 (*26*). In the Y114F mutant no pK_a was apparent (i.e., pK_a > 10). Given that the reduction of Mo(VI) to Mo(V) is coupled with protonation of the oxo ligand to form Mo(V)−OH, the anodic shift in the Y114F mutant coupled with the invariance of the second reduction step to mutation at this position implicates the introduced proton in this process. In rationalizing this observation, the disposition of the coordinated OH^- ligand in the pentavalent complex is critical as it may be both an H-bond donor and acceptor, depending on the orientation of the O−H bond. Given that a significant H-bonding interaction between W116 and the Mo(VI)-coordinated oxo ligand (Mo═O···H−N) has been established crystallographically, we might expect that the same interaction is maintained upon reduction and protonation, i.e., Mo(V)−O(H)···HN, in which case the hydroxo ligand H-atom is most likely directed toward the Y114/F114 residue. Therefore, replacement of the tyrosine hydroxyl group with an H-atom reduces steric H···H repulsion with the Mo(V)-coordinated hydroxo ligand, thus stabilizing the pentavalent form of the enzyme. Electrochemical measurements on the W116 mutant are planned, and these may shed further light on this phenomenon. The importance of Y114 in protolytic reactions associated with enzyme turnover is further reinforced by the observation that the pH optimum for PES-dependent DMS:DCPIP oxidoreductase activity was increased by about 1 pH unit.

ACKNOWLEDGMENT

The authors thank Dr. Sue Bailey for helpful discussions.

REFERENCES

1. Hille, R. (2002) *Trends Biochem. Sci. 27*, 360−367.
2. Hille, R. (1996) *Chem. Rev. 96*, 2757−2816.
3. Kisker, C., Schindelin, H., Baas, D., Retey, J., Meckenstock, R. U., and Kroneck, P. M. (1998) *FEMS Microbiol. Rev. 22*, 503−521.
4. Romao, M. J., Knablein, J., Hüber, R., and Moura, J. J. (1997) *Prog. Biophys. Mol. Biol. 68*, 121−144.
5. McEwan, A. G., Ridge, J. P., McDevitt, C., and Hugenholtz, P. (2002) *Geomicrobiol. J. 19*, 3−21.
6. Schindelin, H., Kisker, C., Hilton, J., Rajagopalan, K. V., and Rees, D. C. (1996) *Science 272*, 1615−1621.
7. Schneider, F., Lowe, J., Hüber, R., Schindelin, H., Kisker, C., and Knablein, J. (1996) *J. Mol. Biol. 263*, 53−69.
8. McAlpine, A. S., McEwan, A. G., Shaw, A. L., and Bailey, S. (1997) *J. Biol. Inorg. Chem. 2*, 690−701.
9. McAlpine, A. S., McEwan, A. G., and Bailey, S. (1998) *J. Mol. Biol. 275*, 613−623.

10. Li, H. K., Temple, C. A., Rajagopalan, K., and Schindelin, H. (2000) *J. Am. Chem. Soc. 122*, 7673−7680.
11. Boyington, J. C., Gladyshev, V. N., Khangulov, S. V., Stadtman, T. C., and Sun, P. D. (1997) *Science 275*, 1305−1308.
12. Dias, J. M., Than, M. E., Humm, A., Hüber, R., Bourenkov, G. P., Bartunik, H. D., Bursakov, S., Calvete, J., Caldeira, J., Carneiro, C., Moura, J. J., Moura, I., and Romao, M. J. (1999) *Struct. Folding Des. 7*, 65−79.
13. Czjzek, M., Dos Santos, J. P., Pommier, J., Giordano, G., Mejean, V., and Haser, R. (1998) *J. Mol. Biol. 284*, 435−447.
14. Ellis, P. J., Conrads, T., Hille, R., and Kuhn, P. (2001) *Structure 9*, 125−132.
15. Johnson, M. K., Garton, S. D., and Oku, H. (1997) *J. Biol. Inorg. Chem. 2*, 797−803.
16. Bell, A. F., He, X., Ridge, J. P., Hanson, G. R., McEwan, A. G., and Tonge, P. J. (2001) *Biochemistry 40*, 440−448.
17. George, G. N., Hilton, J., Temple, C. A., Prince, R. C., and Rajagopalan, K. V. (1999) *J. Am. Chem. Soc. 121*, 1256−1266.
18. Johnson, K. E., and Rajagopalan, K. (2001) *J. Biol. Chem. 276*, 13178−13185.
19. Hilton, J. C., Temple, C. A., and Rajagopalan, K. V. (1999) *J. Biol. Chem. 274*, 8428−8436.
20. Bray, R. C., Adams, B., Smith, A. T., Bennett, B., and Bailey, S. (2000) *Biochemistry 37*, 11258−11269.
21. Shaw, A. L., Leimkuhler, S., Klipp, W., Hanson, G. R., and McEwan, A. G. (1999) *Microbiology 145*, 1409−1420.
22. Hirsch, P. R., and Beringer, J. E. (1984) *Plasmid 12*, 139−141.
23. Penfold, R. J., and Pemberton, J. M. (1992) *Gene 118*, 145−146.
24. Masepohl, B., Klipp, W., and Puhler, A. (1988) *Mol. Gen. Genet. 212*, 27−37.
25. McEwan, A. G., Ferguson, S. J., and Jackson, J. B. (1991) *Biochem. J. 274*, 305−307.
26. Aguey-Zinsou, K.-F., Bernhardt, P. V., McEwan, A. G., and Ridge, J. P. (2002) *J. Biol. Inorg. Chem. 7*, 879−883.
27. King, G. F., Richardson, D. J., Jackson, J. B., and Ferguson, S. J. (1987) *Arch. Microbiol. 149*, 47−51.
28. Solomon, P. S., Shaw, A. L., Lane, I., Hanson, G. R., Palmer, T., and McEwan, A. G. (1999) *Microbiology 145*, 1421−1429.
29. Adams, B., Smith, A. T., Bailey, S., McEwan, A. G., and Bray, R. C. (1999) *Biochemistry 38*, 8501−8511.
30. Bray, R. C., Adams, B., Smith, A. T., Richards, R. L., Lowe, D. J., and Bailey, S. (2001) *Biochemistry 40*, 9810−9820.
31. Sung, K. M., and Holm, R. H. (2001) *J. Am. Chem. Soc. 123*, 1931−1943.
32. Holm, R. H., and Donahue, J. P. (1993) *Polyhedron 12*, 571−589.
33. Webster, C. E., and Hall, M. B. (2001) *J. Am. Chem. Soc. 123*, 5820−5821.

BI0266582